ACS Photonics

pubs.acs.org/journal/apchd5

Article

Critical Role of Low-Energy Protons in Radiation Testing of Perovskite Space Solar Cells

Published as part of ACS Photonics special issue "Rising Stars in Photonics".

Tatchen B. Kum and Ahmad R. Kirmani*

Cite This: https://doi.org/10.1021/acsphotonics.4c01818

Read Online

ACCESS | Metrics & More | Article Recommendations | Supporting Information

ABSTRACT: While perovskite solar cells (PSCs) are attractive for space applications, assessing their radiation tolerance requires adequate testing protocols. The primary criterion is that protons normally incident on a PSC during ground-based testing should create a uniform damage profile, mimicking the effect of the omnidirectional and polyenergetic proton spectrum in space orbit. However, given the low thicknesses of PSCs, proton energies >0.05 MeV can meet this criterion, leading to ambiguity regarding the precise energy needed for testing. Here, we highlight another major criterion: the optimal proton energy should also closely mimic the elemental vacancy distribution created in the perovskite by space protons. Using Monte Carlo ion-solid simulations, we first calculate the elemental vacancies in a PSC due to the low-Earth orbit (LEO) proton spectrum. We then show that only ∼0.07 MeV protons can result in a similar distribution during ground-based testing. Higher energies (∼1 MeV) lead to 25% more iodine, 33% more lead, and 50% fewer hydrogen vacancies, failing to represent the space radiation environment accurately. Our results offer precise guidelines for PSC radiation testing, paving the way for more accurate, reliable, and comparable assessments.

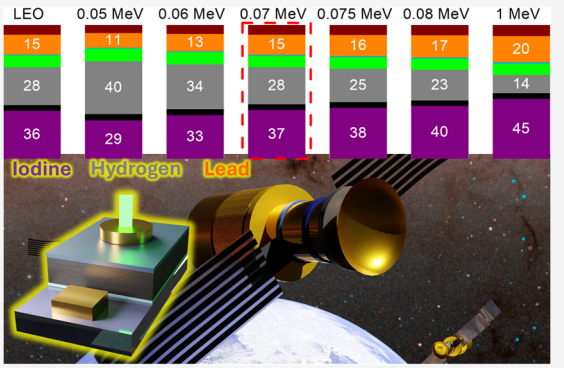

KEYWORDS: *perovskite solar cells, space power, radiation testing, low-energy protons, displacement damage, SRIM simulations*

INTRODUCTION

With the space economy poised for exponential growth, next-generation, low-cost, space-compliant semiconductor technologies are urgently needed. A recent estimate projects the growth of this $630 billion economy as of 2023 to $1.8 trillion by 2035.[1] Spurred by collective interests from private entities and global space agencies, ∼100,000 satellites are expected to be launched and deployed in low-Earth orbit (LEO) over the next decade.[2,3] Higher altitudes of LEO (>1000 km) are of particular interest for the new space age given the lower atmospheric density and reduced risk of deorbiting. In 2022, atmospheric drag in LEO due to a solar storm resulted in the loss of a SpaceX Starlink satellite fleet.[4] Higher altitudes also have less space debris, decreasing the risk of collisions with assets. However, radiation levels increase significantly with altitude, and a 2000 km altitude orbit has ∼3 orders of magnitude higher proton fluences compared to the International Space Station (ISS) orbit at ∼420 km altitude. It is therefore necessary to develop radiation-tolerant semiconductors that can sustain the anticipated proliferation of space.

Interest in exploring perovskite solar cells (PSCs) for space power applications remains strong, fueled by recent developments of >26% AM1.5G power conversion efficiency (PCE) and specific power exceeding 40 $W{\cdot}g^{-1}$.[5−7] Nevertheless, it is critical to establish protocols that can accurately assess their compatibility with the space environment. This is even more important as newer PSC architectures are developed, including tandem device designs.[8−10] Most studies have thus far focused on testing proton radiation tolerance, given the prominence of protons in LEO, which result in a uniform damage profile through the thickness of the device given their polyenergetic spectrum and omnidirectional incidence. These studies highlight that the existing radiation testing standards for traditional space photovoltaics (PVs) are not directly transferrable to PSCs.[11] Recently proposed guidelines emphasize the importance of using low-energy protons (0.05−0.15 MeV) for testing single-junction (1J) PSC device architectures.[11] While higher-energy protons can fully penetrate the PSC and produce a space-like uniform damage profile similar to what is experienced in space, previous work indicates that they might also induce lattice heating.[11−15] This effect may not

Received: September 20, 2024
Revised: November 22, 2024
Accepted: November 26, 2024

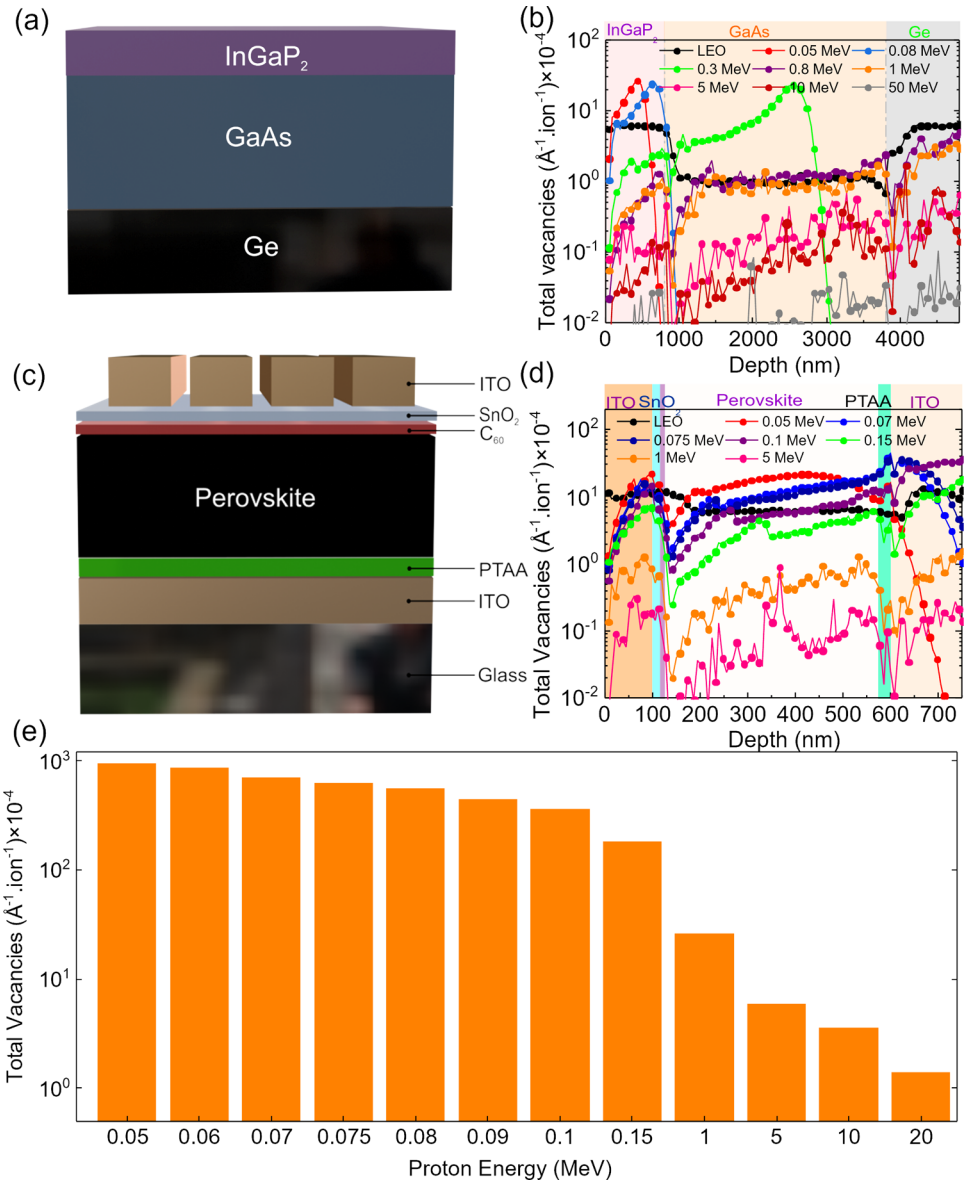

Figure 1. (a) SRIM-simulated proton irradiation of the 3J III−V cell structure from $InGaP_2$ side, (b) total damage profiles produced by various proton energies irradiating the III−V cell, (c) SRIM-simulated proton irradiation of the perovskite cell structure, (d) total damage profiles created by various proton energies irradiating the perovskite cell, and (e) plot showing total vacancies produced in the perovskite layer with increasing proton energy.

accurately represent the near-Earth space environment, where high-energy protons occur at lower fluences. As such, a clear understanding of whether higher energies should be avoided for radiation testing remains to be established. The complex interactions between different proton energies and perovskites, leading to various types of defects,[11,12] suggest that the current guidelines might need reassessment.

In this work, we highlight that while achieving a uniform damage profile during ground-based radiation testing is important, creating an elemental vacancy distribution mimicking space is equally critical. We demonstrate that while fully penetrating protons of energies above 0.8 MeV meet this criterion for III−V solar cells, the situation is more complex for hybrid organic−inorganic PSCs due to their multielement compositions. Using the Monte Carlo ion-solid simulation tool, Stopping Range of Ions in Matter (SRIM), we simulate the elemental vacancies that the LEO proton environment would create in a PSC. Our results show that while protons with energies above 0.05 MeV uniformly penetrate the perovskite layer, only ∼0.07 MeV protons precisely mimic the elemental vacancy distribution seen in space. Despite creating uniform damage profiles, higher-energy protons result in elemental vacancy distributions that do not accurately represent the space environment.

RESULTS AND DISCUSSION

For this study, we considered the LEO at a 2000 km altitude and a medium-Earth orbit (MEO) at a 5000 km altitude. These orbits are particularly important for the new space age, as they offer higher Earth surface coverage for observation and communication and relatively lower atmospheric drag, which can be detrimental to orbiting satellites.[4] For all discussion and figures, LEO here refers to an altitude of 2000 km, 51°

https://doi.org/10.1021/acsphotonics.4c01818
ACS Photonics XXXX, XXX, XXX−XXX

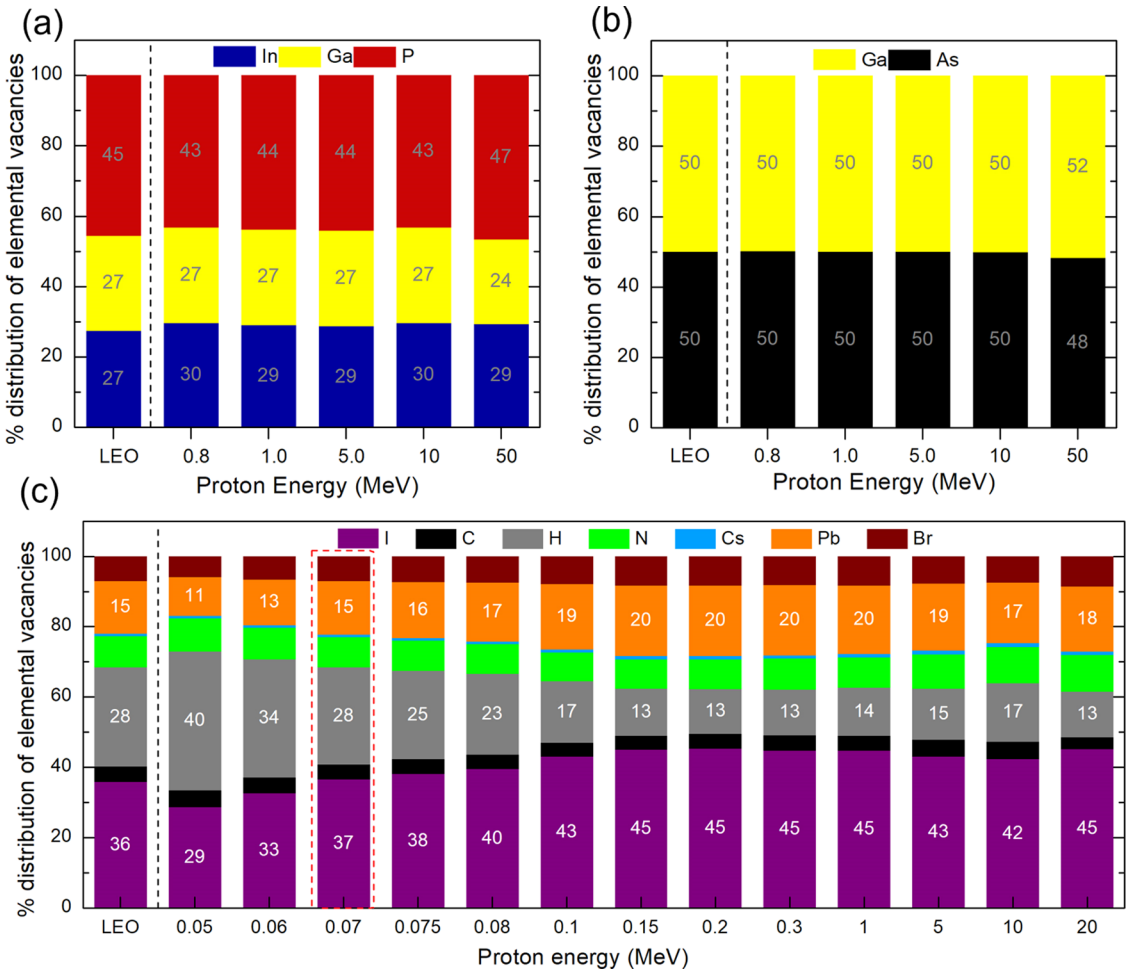

Figure 2. Elemental vacancy distributions due to normally incident proton energies irradiating a III−V cell and PSC, compared to the distribution from the LEO space environment. (a) Top $InGaP_2$ cell, (b) middle GaAs cell of the 3J III−V cell, and (c) triple-cation PIN PSC. For (b), the protons were simulated after passing through the top cell.

inclination, while the MEO refers to a 5000 km 60° inclination orbit.

Uniform Damage Profiles. We began by simulating the interaction of polyenergetic and omnidirectional LEO protons with triple junction (3J) III−V solar cells and PSCs using SRIM (Figure 1). SRIM is a Monte Carlo ion-solid simulation software that tracks the energy losses a proton undergoes while passing through the target.[16] The two losses considered are nonionizing energy loss (NIEL), which is an elastic scattering resulting in atomic displacements and vacancies, and ionizing energy loss (IEL), which is the inelastic scattering with the electrons in the target resulting in ionization. In traditional space power semiconductors, NIEL is the primary loss mechanism and IEL is not known to play a role.[11,17−19] PIN configuration of the PSC was considered given its proven thermal tolerance.[20] The alloyed A-site perovskite chemistry, $Cs_{0.05}(MA_{0.17}FA_{0.83})_{0.95}Pb(I_{0.83}Br_{0.17})_3$, was considered as the active layer with a 0.5 μm thickness. This will be referred to as the "triple-cation" chemistry henceforth. Device architectures considered are shown in Figure 1a,c. The methodology used to simulate LEO proton irradiation is summarized here, with more detailed information in Figure S1. Devices were irradiated from both the front and back sides considering 100,000 protons and averaged. For the back side of the PSC, the metal electrode end, the proton incidence angle was varied from 0 to 89.9° for four distinct proton energies: 0.1, 0.5, 1.0, and 10 MeV weighted by their fluences in the LEO environment. The front indium tin oxide (ITO) glass side irradiation was similarly simulated considering another 100,000 protons, considering a 200 μm thick glass substrate. For the III−V, a 200 μm Ge substrate was considered. This resulted in a slowed proton fluence spectrum, as shown in Figure S2. We considered the average of these two simulations to accurately predict the space damage profiles in the device architectures. These are shown as black curves in Figure 1b,d. The LEO environment results in a uniform damage profile across both the III−V and the perovskite devices. The slight deviation from uniformity in the III−V case is due to the lack of shielding during irradiation from the $InGaP_2$ side, as discussed earlier.[21]

Since ground-based proton radiation testing is most feasible at normal incidence, these scenarios were simulated by using a range of proton energies to determine the energies that would result in a LEO-like uniform damage profile. These damage profiles are plotted in Figure 1b,d. For the III−V device, while the energies below 0.8 MeV do not create the desired uniform damage profile, >0.8 MeV protons fully penetrate the architecture resulting in the LEO-representative profile. These proton energies have therefore been used as a standard

https://doi.org/10.1021/acsphotonics.4c01818
ACS Photonics XXXX, XXX, XXX−XXX

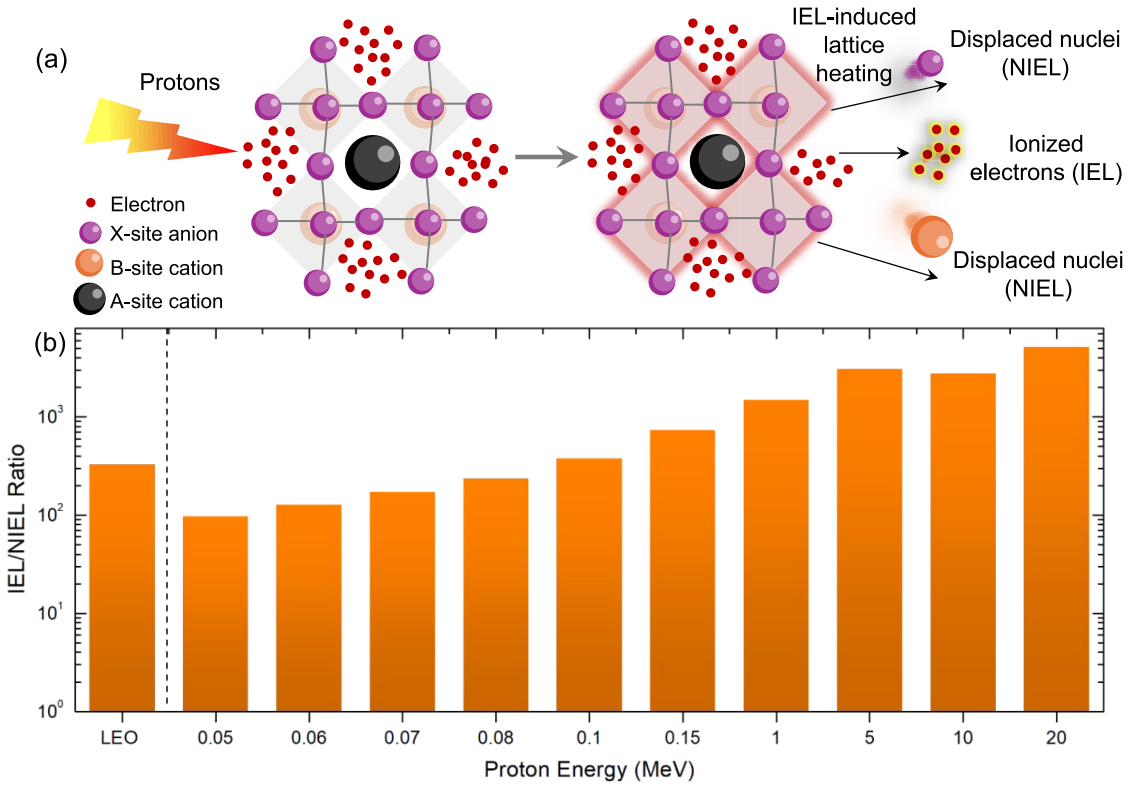

Figure 3. (a) Schematic depicting the interaction of NIEL and IEL with perovskite lattices based on the current understanding. (b) Simulated IEL/NIEL ratio for a triple-cation PSC in the LEO proton environment and upon irradiation with normally incident protons of various energies.

for radiation testing of III−V solar cells, in accordance with the NRL protocols.[17,21]

For PSCs, normally incident protons with energies as low as 0.05 MeV are fully penetrating resulting in a uniform damage profile given the low thickness of the perovskite layer, as previously reported.[11] While higher-energy protons result in lower defects due to reduced NIEL,[11] their fluence can be accordingly increased to achieve the same amount of damage (Figure 1e). In other words, this analysis suggests that all proton energy >0.05 MeV could be used for PSC radiation testing since they enable space-like uniform damage profiles.

Elemental Vacancy Distributions. To resolve this ambiguity in the proton energy range for PSCs, we simulated the resulting elemental vacancies. While achieving a uniform damage profile is an important primary criterion, we argue that it is also important to mimic the elemental vacancy distributions expected in orbit. We considered proton energies in the 0.8−50.0 MeV range for 3J III−V given their full penetration (Figure 1b). While 50.0 MeV protons were included in this analysis, we note that such high energies are present only in negligible fluences in near-Earth orbit environments. More importantly, they can induce unrealistic device performance losses due to nuclear interactions, as highlighted by Warner et al.[22] As such, these high energies are not used for testing the radiation tolerance of space solar cells. Figure 2a,b shows the elemental vacancies resulting from the LEO proton spectrum in the top cell ($InGaP_2$) and middle cell (GaAs). SRIM suggests that LEO protons create 27% In, 27% Ga, and 45% P vacancies in the $InGaP_2$ cell and result in 50% Ga and 50% As vacancies in the GaAs cell. All of the normally incident proton energies result in the same elemental vacancy distributions. This further substantiates the choice of 1−10 MeV protons for the III−V radiation testing.[17,23,24] Energies above 10 MeV are not used since NIEL does not correlate well with displacement damage, with certain other interactions also becoming important.[22]

Figure 2c shows the elemental vacancy distributions for the PSC. The most prominent vacancies created by the LEO protons in the perovskite are 36% I, 28% H, and 15% Pb. Interestingly, only the 0.07 MeV protons are found to result in a similar distribution. While 0.05 MeV protons primarily target the organic framework (C−H, N−H species) leading to significantly higher H vacancies than LEO, >0.07 MeV protons interact strongly with the inorganic (Pb-X) framework resulting in higher I and Pb vacancies.[15,25,26] In fact, I defects are known to act as nonradiative recombination centers contributing to PSC degradation at high proton energies.[26−28] While displacement of Pb atoms can result in metallic Pb trap sites in the perovskite,[29−31] first-principles calculations have also reported that H vacancies from the dissociation of N−H bonds, particularly in methylammonium ($CH_3NH_3^+$)-containing perovskite chemistries, act as nonradiative recombination centers. Such defect-induced charge recombination effects can be minimized through formamidinium ($CH(NH_2)_2^+$) alloying, as this cation exhibits relatively higher dissociation energies for N−H and C−H bonds.[32]

While these simulations were carried out on device architectures with a 0.5 μm thick perovskite absorber, PSCs with absorbers thicker than 0.5 μm are also commonly reported.[33] We simulated radiation effects in a PIN PSC stack with a 1 μm thick absorber. We note that while slightly higher proton energies are needed for full penetration in this architecture, the overall trend remains similar to the LEO environment being closely mimicked by proton energies around 0.1 MeV (Figure S3). This analysis highlights the need to adjust the incident proton energy during ground-based

https://doi.org/10.1021/acsphotonics.4c01818
ACS Photonics XXXX, XXX, XXX−XXX

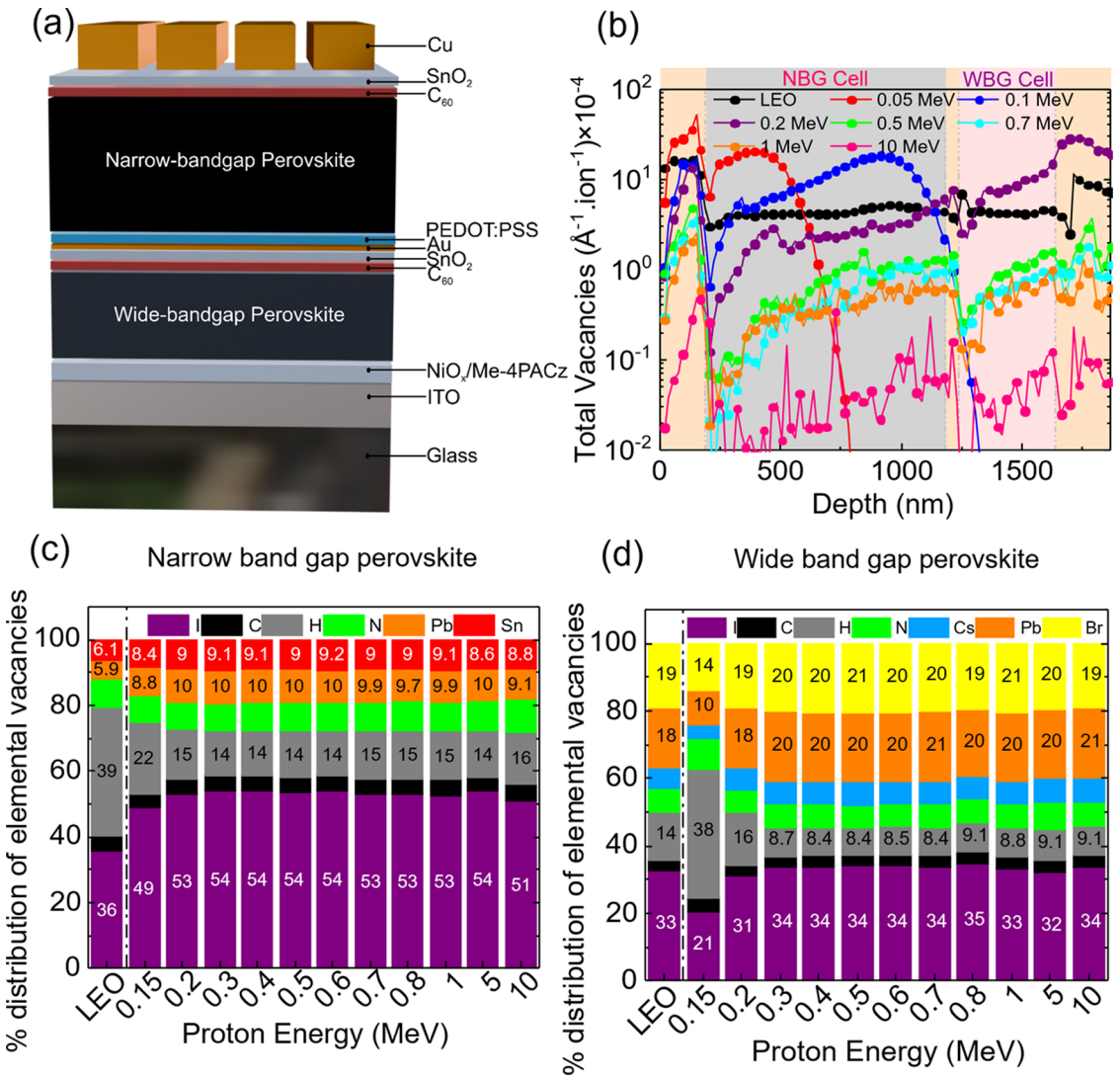

Figure 4. (a) Device schematic of the 2J all-perovskite tandem cell; (b) simulated damage profiles for various proton energy scenarios compared to a uniform damage profile in LEO (black). Elemental vacancies created by LEO and by normally incident protons in (c) the NBG cell and (d) the WBG cell.

testing based on the perovskite absorber thickness and device architecture, such as the presence of barrier layers. This is because the penetration depth of protons increases with energy. A higher proton energy (0.1 MeV) is required to fully penetrate the thicker device stack involving a 1 μm thick perovskite layer.

Energy Loss Modes. As mentioned above, an incident proton undergoes NIEL and IEL as it passes through matter (Figure 3a). The IEL/NIEL ratio is important for PSCs given the soft lattice nature of perovskites and the possibility of IEL-induced healing.[13,25,26] Figure S4a,b depicts the NIEL and IEL profiles for the SRIM-simulated PSC. Figure S4c shows a quantitative analysis of the NIEL and IEL profiles for the LEO and 0.07 MeV protons within the PSC, with comparable displacements and ionizing energy losses. As proton energy increases, NIEL decreases, while IEL increases, resulting in a higher IEL/NIEL ratio, as shown in Figure 3b. A comparison with the IEL/NIEL ratio for LEO implies that only low-energy protons have a space-representative ratio. This suggests that during ground-based radiation testing, normally incident low-energy protons can replicate the IEL effects in a PSC that are expected during a LEO mission.

We believe that the hybrid organic−inorganic nature of the triple-cation perovskite chemistry influences the proton energy dependence of elemental vacancy distributions. As Figure S5 shows, a similar trend is observed for the "double-cation" perovskite chemistry, $FA_{0.88}Cs_{0.12}Pb(I_{0.92}Br_{0.08})_3$, with the LEO closely matched by 0.07 MeV protons. In chemistries lacking this atomic diversity, defects may be independent of proton energy, as observed in III−V semiconductors. Figure S6a,b shows SRIM simulations for an all-inorganic $CsPbI_2Br$ PSC, where protons with energies above 0.05 MeV fully penetrate the perovskite layer, leading to a space-like elemental vacancy distribution, regardless of proton energy. It might appear that for such PSCs all proton energies greater than 0.05 MeV can be used for radiation testing. However, the optimal testing conditions must also replicate the energy loss mechanisms encountered in space environments. Figure S6c illustrates that for $CsPbI_2Br$, only low-energy protons reproduce an IEL/NIEL ratio similar to that found in LEO. Therefore, the IEL/NIEL ratio is an essential criterion for selecting the most

https://doi.org/10.1021/acsphotonics.4c01818
ACS Photonics XXXX, XXX, XXX−XXX

suitable proton energy, particularly in cases where higher energies do not yield distinct displacement distributions.

We explored the generality of low-energy protons for another class of near-Earth orbitals, the medium-Earth orbits (MEOs). These are circular orbits beyond LEO, at a 5000 km altitude with a 60° inclination. These provide broader coverage and are ideal for communication in remote areas, enhanced defense systems, and Global Positioning System (GPS) navigation.[34,35] While MEOs are less affected by atmospheric drag and satellite loss compared to LEOs, they present even greater radiation challenges (Figure S2b). To understand the role of low-energy protons, we simulated proton interactions in PSCs for an MEO mission. As shown in Figure S7, 0.07 MeV protons were found to closely match the vacancies created in a MEO environment.

2J All-Perovskite Tandem Cell Architecture. 2J all-perovskite tandem solar cells promise PCEs beyond single-junction cells and are being rigorously researched with the latest report of >28% PCE.[36,37] While significant work is needed to access their suitability for space applications, we extended our analysis to a 2J architecture to ascertain an appropriate proton energy range for radiation testing. Our analysis highlights the complications associated with simulating proton interactions in such a stack. This architecture involved $FA_{0.7}MA_{0.3}Pb_{0.5}Sn_{0.5}I_3$ chemistry as the narrow band-gap (NBG) cell and $Cs_{0.35}FA_{0.65}PbI_{1.8}Br_{1.2}$ wide-band-gap (WBG) cell.[38] Figure 4a shows the cell stack with a 1 μm NBG cell and 0.4 μm WBG cell. The LEO proton environment creates a uniform damage profile throughout the tandem stack (Figure 4b). However, normally incident low-energy protons below 0.2 MeV led to a nonuniform profile that was not representative of the LEO profile. Energies of ≥0.2 MeV create the desired uniform profile. The corresponding NIEL and IEL profiles are shown in Figure S8.

To further narrow the search for the optimal proton energy, we simulated the elemental vacancy distributions in the subcells (Figure 4c,d). While energies below 0.15 MeV could mimic the LEO vacancies in the NBG cell, these protons would not penetrate the WBG cell, as mentioned above. Protons with energies above 0.15 MeV were not found to mimic LEO vacancies in the NBG cell (Figure 4c). For the vacancy distributions shown in Figure 4d, the protons were simulated to pass through the NBG cell, as expected during radiation testing of a tandem device stack. The low I vacancy content for 0.15 MeV is due to energy downshifting and subsequent stoppage of these protons within the WBG cell, as shown in Figure 4b. We note that 0.2 MeV protons recreate LEO distribution in the WBG cell while failing to do in the NBG cell. This analysis suggests that a true radiation assessment of tandem solar cells is complicated due to two separate perovskite subcells and each subcell might need to be irradiated separately. This situation was not encountered in a 3J III−V stack discussed in the beginning, given the chemical simplicity of those subcell compositions.

We note that the irradiation of PSCs and tandems with proton energies lower and higher than 0.07 MeV is relevant to developing a mechanistic understanding of radiation defects and to exploring the wide variety of defect types. In fact, higher-energy protons can selectively target iodine and lead vacancies, while lower-energy protons preferentially induce hydrogen vacancies. Protons in the energy range of 10−30 keV can be used to probe interfaces via targeted damage. Additionally, a recent theoretical analysis has highlighted the importance of hydrogen vacancies in methylammonium and formamidinium lead iodide perovskites.[32] While damage to the methylammonium A-site organic cation has been thought to be irrelevant to the overall charge transport given the unique band structure of MHPs governed by the inorganic PbX_3 network, it was shown that $CH_3NH_3^+$ could undergo H loss resulting in $CH_3NH_2^+$ (methylamine), a nonradiative recombination center. The study also found that H vacancies are more difficult to form with formamidinium (FA = $CH(NH_2)_2$) at the A-site.[32] Proton irradiation with various energies discussed in our study can be useful to experimentally confirm these predictions.

CONCLUSIONS

The main finding of this work is that low-energy protons, specifically with an energy of 0.07 MeV, most closely mimic the effects of space radiation on perovskite solar cells during a near-Earth orbit mission. These protons result in a uniform damage profile, replicate the elemental vacancy distribution, and lead to similar energy losses inside the perovskite, as would be expected in near-Earth space conditions. Our study narrows the testing energy range and emphasizes that achieving a uniform damage profile alone is insufficient. Given the chemical complexity of perovskites, optimal proton energies for radiation testing must consider the specific interactions of each element.

METHODS

SPENVIS Calculations. Before performing the SRIM Monte Carlo program[39] simulations, the desired orbits were created in the Space Environment Information System (SPENVIS).[40] SPENVIS is a software developed by the European Space Agency and uses the standard AP-8 and AE-8 NASA models for predicting trapped proton and electron environments for Earth orbits. The following information parameters were used for the two orbits:

LEO (circular orbit): altitude; 2000 km, inclination; 51.0°, argument of perigee; 42.17°, true anomaly; 130.61°.

MEO (circular orbit): altitude 5000 km, inclination; 60.0°, argument of perigee and anomaly are the same as for the LEO case.

Stopping Range of Ions in Matter (SRIM) Simulations. SRIM[39] simulations were performed employing the "detailed calculation with full damage cascades" TRIM calculation mode considering a total of 100,000 protons or α particles irradiating a PIN device architecture. The irradiated PIN device stack consists of ITO (100 nm)/SnO_2 (15 nm)/C_{60} (10 nm)/perovskite (450 nm)/PTAA (25 nm)/ITO (150 nm)/glass (200 μm). The densities used for different layers were ITO = 7.20 g·cm^{-3}, Au = 19.31 g·cm^{-3}, Cu = 8.92 g·cm^{-3}, SnO_2 = 6.95 g·cm^{-3}, C_{60} = 1.65 g·cm^{-3}, $Cs_{0.05}(MA_{0.17}FA_{0.83})_{0.95}Pb(I_{0.83}Br_{0.17})_3$ = 4.3 g·cm^{-3}, $CsPbI_2Br$ = 4.03 g·cm^{-3}, $Cs_{0.35}FA_{0.65}PbI_{1.8}Br_{1.2}$ = 4.55 g·cm^{-3}, $FA_{0.7}MA_{0.3}Pb_{0.5}Sn_{0.5}I_3$ = 3.84 g·cm^{-3}, PTAA = 1.4 g·cm^{-3}, NiO_x = 6.67 g·cm^{-3}, PEDOT:PSS = 1.011 g·cm^{-3}, Me-4PACz = 1 g·cm^{-3}, and glass = 2.53 g·cm^{-3}. The SRIM displacement energies were used unchanged; H = 10 eV, C = 28 eV, N = 28 eV, and O = 28 eV, Cs = 25 eV, Pb = 25 eV, I = 25 eV, Br = 25 eV, In = 25 eV, Sn = 25 eV, Ge = 15 eV, P = 25 eV, As = 25 eV, and Ga = 25 eV.

https://doi.org/10.1021/acsphotonics.4c01818
ACS Photonics XXXX, XXX, XXX−XXX

■ ASSOCIATED CONTENT

Supporting Information

The Supporting Information is available free of charge at https://pubs.acs.org/doi/10.1021/acsphotonics.4c01818.

SPENVIS simulations on proton spectrum for LEO and MEO, polyenergetic/omnidirectional SRIM simulations for these orbits, SRIM simulations for $CsPbI_2Br$ and double-cation perovskite device architectures, and SRIM simulations for a PSC with a 1 μm thick perovskite layer (PDF)

■ AUTHOR INFORMATION

Corresponding Author

Ahmad R. Kirmani − *School of Chemistry and Materials Science, Rochester Institute of Technology, Rochester, New York 14623, United States; Microsystems Engineering and NanoPower Research Laboratories, Rochester Institute of Technology, Rochester, New York 14623, United States;* orcid.org/0000-0002-8351-3762; Email: ahmad.kirmani@rit.edu

Author

Tatchen B. Kum − *School of Chemistry and Materials Science, Rochester Institute of Technology, Rochester, New York 14623, United States; Microsystems Engineering and NanoPower Research Laboratories, Rochester Institute of Technology, Rochester, New York 14623, United States;* orcid.org/0009-0001-3918-990X

Complete contact information is available at: https://pubs.acs.org/10.1021/acsphotonics.4c01818

Notes

The authors declare no competing financial interest.

■ ACKNOWLEDGMENTS

The authors acknowledge ongoing support from the College of Science and the School of Chemistry and Materials Science from the Rochester Institute of Technology. T.B.K. acknowledges support from the Dr. Russell and Melissa Bessette Award for Doctoral Student Excellence.

■ REFERENCES

(1) Space: The $1.8 Trillion Opportunity for Global Economic Growth; World Economic Forum, 2024. https://www.weforum.org/publications/space-the-1-8-trillion-opportunity-for-global-economic-growth/ (accessed Aug 02, 2024).

(2) Mediavilla, D. 100,000 Satellites Over head: The New Race to make Access to Space an Everyday Occurrence; EL PAÍS English. https://english.elpais.com/technology/2024-02-24/100000-satellites-overhead-the-new-race-to-make-access-to-space-an-everyday-occurrence.html (accessed Mar 18, 2024).

(3) Zhang, J.; Cai, Y.; Xue, C.; Xue, Z.; Cai, H. LEO Mega Constellations: Review of Development, Impact, Surveillance, and Governance. *Space: Sci. Technol.* **2022**, *2022*, No. 9865174.

(4) Berger, T. E.; Dominique, M.; Lucas, G.; Pilinski, M.; Ray, V.; Sewell, R.; Sutton, E. K.; Thayer, J. P.; Thiemann, E. The Thermosphere Is a Drag: The 2022 Starlink Incident and the Threat of Geomagnetic Storms to Low Earth Orbit Space Operations. *Space Weather* **2023**, *21* (3), No. e2022SW003330.

(5) Kang, S.; Jeong, J.; Cho, S.; Yoon, Y. J.; Park, S.; Lim, S.; Kim, J. Y.; Ko, H. Ultrathin, Lightweight and Flexible Perovskite Solar Cells with an Excellent Power-per-Weight Performance. *J. Mater. Chem. A* **2019**, *7* (3), 1107−1114.

(6) Kaltenbrunner, M.; Adam, G.; Głowacki, E.; Drack, M.; Schwödiauer, R.; Leonat, L.; Apaydin, D.; Groiss, H.; Scharber, M.; White, M.; Sariciftci, N.; Bauer, S. Flexible High Power-per-Weight Perovskite Solar Cells with Chromium Oxide-Metal Contacts for Improved Stability in Air. *Nat. Mater.* **2015**, *14*, 1032−1039.

(7) Hailegnaw, B.; Demchyshyn, S.; Putz, C.; Lehner, L. E.; Mayr, F.; Schiller, D.; Pruckner, R.; Cobet, M.; Ziss, D.; Krieger, T. M.; Rastelli, A.; Sariciftci, N. S.; Scharber, M. C.; Kaltenbrunner, M. Flexible Quasi-2D Perovskite Solar Cells with High Specific Power and Improved Stability for Energy-Autonomous Drones. *Nat. Energy* **2024**, *9*, 677.

(8) Lang, F.; Eperon, G. E.; Frohna, K.; Tennyson, E. M.; Al-Ashouri, A.; Kourkafas, G.; Bundesmann, J.; Denker, A.; West, K. G.; Hirst, L. C.; Neitzert, H.-C.; Stranks, S. D. Proton-Radiation Tolerant All-Perovskite Multijunction Solar Cells. *Adv. Energy Mater.* **2021**, *11* (41), No. 2102246.

(9) Lang, F.; Jošt, M.; Frohna, K.; Köhnen, E.; Al-Ashouri, A.; Bowman, A. R.; Bertram, T.; Morales-Vilches, A. B.; Koushik, D.; Tennyson, E. M.; Galkowski, K.; Landi, G.; Creatore, M.; Stannowski, B.; Kaufmann, C. A.; Bundesmann, J.; Rappich, J.; Rech, B.; Denker, A.; Albrecht, S.; Neitzert, H.-C.; Nickel, N. H.; Stranks, S. D. Proton Radiation Hardness of Perovskite Tandem Photovoltaics. *Joule* **2020**, *4* (5), 1054−1069.

(10) Yoon, G. W.; Jo, B.; Boonmongkolras, P.; Han, G. S.; Jung, H. S. Perovskite Tandem Solar Cells for Low Earth Orbit Satellite Power Applications. *Adv. Energy Mater.* **2024**, No. 2400204.

(11) Kirmani, A. R.; Durant, B. K.; Grandidier, J.; Haegel, N. M.; Kelzenberg, M. D.; Lao, Y. M.; McGehee, M. D.; McMillon-Brown, L.; Ostrowski, D. P.; Peshek, T. J.; Rout, B.; Sellers, I. R.; Steger, M.; Walker, D.; Wilt, D. M.; VanSant, K. T.; Luther, J. M. Countdown to Perovskite Space Launch: Guidelines to Performing Relevant Radiation-Hardness Experiments. *Joule* **2022**, *6* (5), 1015−1031.

(12) Lang, F.; Jošt, M.; Bundesmann, J.; Denker, A.; Albrecht, S.; Landi, G.; Neitzert, H.-C.; Rappich, J.; Nickel, N. H. Efficient Minority Carrier Detrapping Mediating the Radiation Hardness of Triple-Cation Perovskite Solar Cells under Proton Irradiation. *Energy Environ. Sci.* **2019**, *12* (5), 1634−1647.

(13) Durant, B. K.; Afshari, H.; Singh, S.; Rout, B.; Eperon, G. E.; Sellers, I. R. Tolerance of Perovskite Solar Cells to Targeted Proton Irradiation and Electronic Ionization Induced Healing. *ACS Energy Lett.* **2021**, *6* (7), 2362−2368.

(14) Khanal, M. N.; Whiteside, V. R.; Parashar, M.; Merckx, T.; Sharma, M.; Kuang, Y.; Aguirre, A.; Afshari, H.; Hamtaei, S.; Aernouts, T.; Vermang, B.; Rout, B.; Sellers, I. R. Radiation versus Environmental Degradation in Unencapsulated Metal Halide Perovskite Solar Cells. *J. Phys.: Energy* **2024**, *6*, No. 045001, DOI: 10.1088/2515-7655/ad658d.

(15) Afshari, H.; Chacon, S. A.; Sourabh, S.; Byers, T. A.; Whiteside, V. R.; Crawford, R.; Rout, B.; Eperon, G. E.; Sellers, I. R. Radiation Tolerance and Self-Healing in Triple Halide Perovskite Solar Cells. *APL Energy* **2023**, *1* (2), No. 026105.

(16) Ziegler, J. F.; Ziegler, M. D.; Biersack, J. P. SRIM − The Stopping and Range of Ions in Matter (2010). *Nucl. Instrum. Methods Phys. Res., Sect. B* **2010**, *268* (11), 1818−1823.

(17) Messenger, S. R.; Summers, G. P.; Burke, E. A.; Walters, R. J.; Xapsos, M. A. Modeling Solar Cell Degradation in Space: A Comparison of the NRL Displacement Damage Dose and the JPL Equivalent Fluence Approaches. *Prog. Photovoltaics* **2001**, *9* (2), 103−121.

(18) Anspaugh, B. E. GaAs Solar Cell Radiation Handbook; NASA-CR-203421, 1996. https://ntrs.nasa.gov/citations/19970010878 (accessed Apr 02, 2024).

(19) Weaver, B. D.; Walters, R. J. Displacement Damage Effects in Electronic and Optoelectronic Devices. *Recent Res. Dev. Appl. Phys.* **2003**, *6*, 747−776.

(20) VanSant, K. T.; Kirmani, A. R.; Patel, J. B.; Crowe, L. E.; Ostrowski, D. P.; Wieliczka, B. M.; McGehee, M. D.; Schelhas, L. T.; Luther, J. M.; Peshek, T. J.; McMillon-Brown, L. Combined Stress

Testing of Perovskite Solar Cells for Stable Operation in Space. *ACS Appl. Energy Mater.* **2023**, *6* (20), 10319−10326.
(21) Messenger, S. R.; Burke, E. A.; Walters, R. J.; Warner, J. H.; Summers, G. P.; Morton, T. L. Effect of Omnidirectional Proton Irradiation On Shielded Solar Cells. *IEEE Trans. Nucl. Sci.* **2006**, *53* (6), 3771−3778.
(22) Warner, J. H.; Walters, R. J.; Messenger, S. R.; Summers, G. P.; Khanna, S. M.; Estan, D.; Erhardt, L. S.; Houdayer, A. High-Energy Proton Irradiation Effects in GaAs Devices. *IEEE Trans. Nucl. Sci.* **2004**, *51* (5), 2887−2895.
(23) Messenger, S. R.; Xapsos, M. A.; Burke, E. A.; Walters, R. J.; Summers, G. P. Proton Displacement Damage and Ionizing Dose for Shielded Devices in Space. *IEEE Trans. Nucl. Sci.* **1997**, *44* (6), 2169−2173.
(24) Summers, G. P.; Messenger, S. R.; Burke, E. A.; Xapsos, M. A.; Walters, R. J. Low Energy Proton-Induced Displacement Damage in Shielded GaAs Solar Cells in Space. *Appl. Phys. Lett.* **1997**, *71* (6), 832−834.
(25) Brus, V. V.; Lang, F.; Bundesmann, J.; Seidel, S.; Denker, A.; Rech, B.; Landi, G.; Neitzert, H. C.; Rappich, J.; Nickel, N. H. Defect Dynamics in Proton Irradiated CH3NH3PbI3 Perovskite Solar Cells. *Adv. Electron. Mater.* **2017**, *3* (2), No. 1600438.
(26) Kirmani, A. R.; Byers, T. A.; Ni, Z.; VanSant, K.; Saini, D. K.; Scheidt, R.; Zheng, X.; Kum, T. B.; Sellers, I. R.; McMillon-Brown, L.; Huang, J.; Rout, B.; Luther, J. M. Unraveling Radiation Damage and Healing Mechanisms in Halide Perovskites Using Energy-Tuned Dual Irradiation Dosing. *Nat. Commun.* **2024**, *15* (1), No. 696.
(27) Zhang, X.; Turiansky, M.; Shen, J.-X.; Van de Walle, C. Iodine Interstitials as a Cause of Nonradiative Recombination in Hybrid Perovskites. *Phys. Rev. B* **2020**, *101*, No. 140101, DOI: 10.1103/PhysRevB.101.140101.
(28) Uddin, M. A.; Rana, P. J. S.; Ni, Z.; Yang, G.; Li, M.; Wang, M.; Gu, H.; Zhang, H.; Dou, B. D.; Huang, J. Iodide Manipulation Using Zinc Additives for Efficient Perovskite Solar Minimodules. *Nat. Commun.* **2024**, *15* (1), No. 1355.
(29) Kirmani, A. R.; Mansour, A. E.; Yang, C.; Munir, R.; El-Zohry, A. M.; Mohammed, O. F.; Amassian, A. Facile and Noninvasive Passivation, Doping and Chemical Tuning of Macroscopic Hybrid Perovskite Crystals. *PLoS One* **2020**, *15* (3), No. e0230540.
(30) Liang, J.; Hu, X.; Wang, C.; Liang, C.; Chen, C.; Xiao, M.; Li, J.; Tao, C.; Xing, G.; Yu, R.; Ke, W.; Fang, G. Origins and Influences of Metallic Lead in Perovskite Solar Cells. *Joule* **2022**, *6* (4), 816−833.
(31) Jin, B.; Zhao, D.; Liang, F.; Liu, L.; Liu, D.; Wang, P.; Qiu, M. Electron-Beam Irradiation Induced Regulation of Surface Defects in Lead Halide Perovskite Thin Films. *Research* **2021**, *2021*, No. 9797058.
(32) Zhang, X.; Shen, J.-X.; Turiansky, M. E.; Van de Walle, C. G. Minimizing Hydrogen Vacancies to Enable Highly Efficient Hybrid Perovskites. *Nat. Mater.* **2021**, *20* (7), 971−976.
(33) Chen, M.; Dong, Y.; Zhang, Y.; Zheng, X.; McAndrews, G. R.; Dai, Z.; Jiang, Q.; You, S.; Liu, T.; Harvey, S. P.; Zhu, K.; Oliveto, V.; Jackson, A.; Witteck, R.; Wheeler, L. M.; Padture, N. P.; Dyson, P. J.; McGehee, M. D.; Nazeeruddin, M. K.; Beard, M. C.; Luther, J. M. Stress Engineering for Mitigating Thermal Cycling Fatigue in Perovskite Photovoltaics. *ACS Energy Lett.* **2024**, *9* (6), 2582−2589.
(34) Johnson—MEDIUM EARTH ORBITS IS THERE A NEED FOR A THIRD P.Pdf. https://ntrs.nasa.gov/api/citations/20100007939/downloads/20100007939.pdf (accessed June 20, 2024).
(35) Medium Earth Orbit (MEO) Satellite Constellations|SES. https://www.ses.com/o3b-mpower/power-meo (accessed June 20, 2024).
(36) Lim, J.; Park, N.-G.; Il Seok, S.; Saliba, M. All-Perovskite Tandem Solar Cells: From Fundamentals to Technological Progress. *Energy Environ. Sci.* **2024**, *17* (13), 4390−4425.
(37) Pan, Y.; Wang, J.; Sun, Z.; Zhang, J.; Zhou, Z.; Shi, C.; Liu, S.; Ren, F.; Chen, R.; Cai, Y.; Sun, H.; Liu, B.; Zhang, Z.; Zhao, Z.; Cai, Z.; Qin, X.; Zhao, Z.; Ji, Y.; Li, N.; Huang, W.; Liu, Z.; Chen, W. Surface Chemical Polishing and Passivation Minimize Non-Radiative Recombination for All-Perovskite Tandem Solar Cells. *Nat. Commun.* **2024**, *15* (1), No. 7335.
(38) Gao, H.; Xiao, K.; Lin, R.; Zhao, S.; Wang, W.; Dayneko, S.; Duan, C.; Ji, C.; Sun, H.; Bui, A. D.; Liu, C.; Wen, J.; Kong, W.; Luo, H.; Zheng, X.; Liu, Z.; Nguyen, H.; Xie, J.; Li, L.; Saidaminov, M. I.; Tan, H. Homogeneous Crystallization and Buried Interface Passivation for Perovskite Tandem Solar Modules. *Science* **2024**, *383* (6685), 855−859.
(39) James Ziegler - SRIM & TRIM. http://www.srim.org/ (accessed June 08, 2024).
(40) SPENVIS - Space Environment, Effects, and Education System. https://www.spenvis.oma.be/ (accessed June 08, 2024).

https://doi.org/10.1021/acsphotonics.4c01818
ACS Photonics XXXX, XXX, XXX−XXX